UCRL 13660

GTE

TR 75-029.1

UC 25
70 c l c 2

FLUORESCENCE LINE-NARROWING STUDIES OF Nd:GLASS LASER MATERIALS

by

L.A. Riseberg and C. Brecher

Contract No. W-7405-Eng. 48
P.O. 5236705

FINAL REPORT

Submitted to

LAWRENCE LIVERMORE LABORATORY
Livermore, California

GTE LABORATORIES INCORPORATED
Waltham, Massachusetts 02154

TR 75-029.1

FLUORESCENCE LINE-NARROWING STUDIES OF Nd:GLASS LASER MATERIALS

by

L.A. Riseberg
C. Brecher

Contract No. W-7405-Eng. 48

FINAL REPORT

Submitted to

LAWRENCE LIVERMORE LABORATORY
Livermore, California 94550

GTE LABORATORIES INCORPORATED
40 Sylvan Road
Waltham, Massachusetts 02154

PRINTED IN USA

TABLE OF CONTENTS

LIST OF ILLUSTRATIONS

1. INTRODUCTION

The optical properties of magnetic ions in glasses represent a major frontier in solid state spectroscopy. Because of the distribution of environments seen by rare earth dopants in glassy media, the observed spectra are superpositions of contributions over a large range of microscopic conditions. This is to be compared with ions in crystals where the spectroscopist observes only a single class of sites. The elegant and powerful analytical techniques developed for crystalline systems are not immediately applicable in the case of amorphous solids.

The increasing importance of Nd glass lasers in laser fusion technology has emphasized the inadequacy in the understanding of the optical properties of rare earth ions in glasses. Indeed, it has been difficult to generate models for the performance of these devices, and the selection of host glasses could be done by little more than a trial-and-error approach.

The technique of laser-induced fluorescence line-narrowing developed within the last few years provides a new and powerful tool for the study of these systems. In this technique, a laser excites within the inhomogeneously broadened absorption bands a selected subgroup of the ions in the system, namely those whose absorption energy is resonant with the laser. If the excitation does not migrate among the entire collection of ions prior to fluorescence, the fluorescence that is observed is only from the group that was excited and is narrowed. This permits the selective study of classes of ion sites within the ensemble. The concept is indicated schematically in Figure 1. By the use of a tunable laser, such as a dye laser, it is possible to vary the class of sites, defined by energy, that is excited and thereby study the important spectroscopic properties and their variations, unclouded by the averaging that occurs under excitation of the entire system. Furthermore, it is then possible to use the spectroscopic information to infer a description of the variation of the microscopic environment, and a rationalization of the effects of compositional changes. Use of a pulsed dye laser and time-resolved detection permits the study of the dynamics, including, for example, the energy transfer among ions of different energies within the inhomogeneously-broadened spectrum.

The goal of this project has been to apply such studies to glasses of interest to glass laser technology, providing information for device modeling, and establishing design criteria for glass selection.

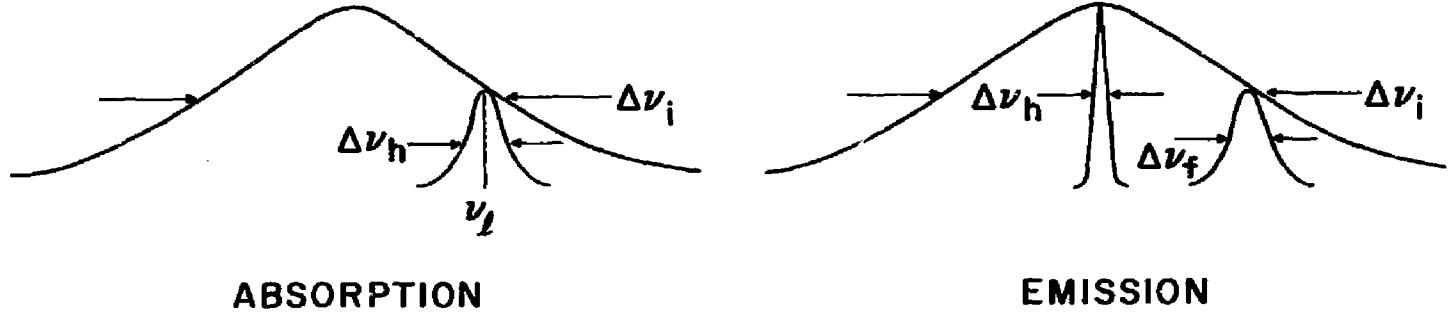

Figure 1. Concept of Laser-Induced Fluorescence Line-Narrowing. Within the inhomogenously broadened absorption line, width $\Delta\nu_i$, the laser line ν_ℓ selectively excites a subset of ions determined by the laser wavelength and the homogeneous width $\Delta\nu_h$ characteristic of the transition. The inhomogeneously broadened emission, width $\Delta\nu_i$, consists of a distribution of emissions of homogeneous width $\Delta\nu_h$. The width $\Delta\nu_f$ of the fluorescence is a convolution of the two homogeneous widths.

Early in the course of the project it was determined that the unique characteristics of the Eu^{3+} ion were ideal for the initial thrust, and a detailed FLN study was carried out for a barium sodium zinc silicate glass doped with Eu^{3+}. Excitation within the $^7F_0 \rightarrow {}^5D_0$ transition was accomplished with a Rhodamine 6G dye laser, while observations were made of the $^5D_0 \rightarrow {}^7F_1$ and $^5D_0 \rightarrow {}^7F_2$ fluorescences. Variations of the crystal field splittings were determined for the terminal levels, and the distribution of crystal field parameters within the glass were extracted. These were used to generate a model for the variation in microstructure within the glass, involving a distortion from eight-fold to nine-fold coordination. Furthermore, the variation in lifetime and linewidth has been studied across the inhomogeneously broadened spectrum.

The experimental study was extended to two additional Eu^{3+}-containing glasses, high-lithia phosphate and silicate analogues. An attempt will be made to delineate the microscopic changes introduced by the change in the basic glass constituent. The experimental results appear promising and the analysis is under way.

2. EXPERIMENTAL TECHNIQUE

The basic tool for laser-induced fluorescence line-narrowing experiments is the tunable dye laser. In the studies reported here an Avco Model C950 pulsed N_2 laser is used for dye laser pumping. The geometry of the experimental arrangement is shown in Figure 2. The dye cell is wedged to minimize undesirable residual feedback from the surfaces of the cell-windows. A Tropel collimator with coated optics is used intra-cavity with a PTR echelle grating. This arrangement provides a dye laser output in a single line less than 0.5Å wide, as shown in Figure 3. The output pulse of the dye laser with Rb 6G 10^{-3} M in ethanol is about 10 Kw in peak power and 15 ns long. Typical operating repetition rate was 10-20 Hz. A Janis Vari-Temp cryostat provided stable temperatures down to 15 K. Both side and rear illumination were used, depending on the requirements of the experiment.

Electronically gated detection was provided by a PAR Model 160 Boxcar Averager, triggered by the laser. Short delays after excitation provided the capability for observation prior to cross-relaxation to maximize the line-narrowed component of the emission, while spectra at different delays provided information about the cross-relaxation itself. Scanning of the delay also was used in signal averaging for lifetime measurements, although in certain cases the lifetime measurements were made with a PAR TDH-9 waveform eductor.

Signal-to-noise characteristics of the system were excellent, with the major limitation coming from scattered laser light under conditions of close approach to the laser pulse either in time or wavelength.

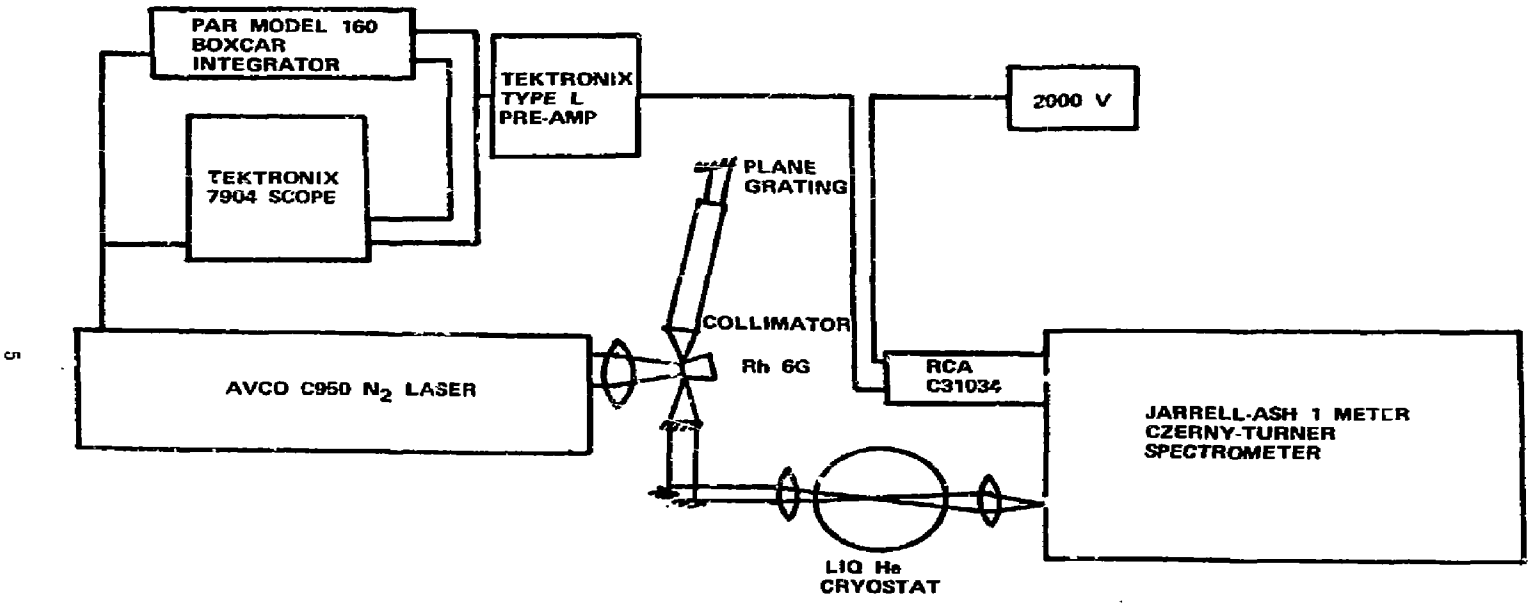

Figure 2. Experimental Apparatus for Laser-Induced Fluorescence Line-Narrowing Measurements

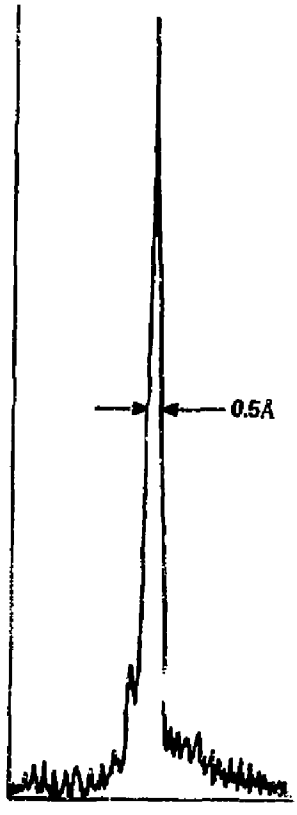

Figure 3. Typical Shape of the Tuned Dye Laser Line

2. NBS L-20 AND L-II Eu^{3+} DOPED GLASSES

The bulk of the analytical work that was carried out under this program involved the line-narrowed spectra obtained under $^5D_0 - ^7D_0$ excitation of Eu^{3+} in a barium sodium zinc silicate glass fabricated by NBS and provided to us by LLL for study. Only a brief discussion of these results will be presented here. A full treatment has been prepared as a paper for publication and is included as an appendix.

Striking line-narrowing behavior is observed for the $^5D_0 - ^7F_0$ and $^5D_0 - ^7F_2$ transitions. By scanning of the excitation wavelength, it was possible to observe the spectra over the entire range of ion sites found in the glass. A crystal field analysis was carried out on these spectra. The crystal field variation was rationalized against a model for the change in the microscopic structure, involving a gradual transition from eight-fold to nine-fold coordination at the rare-earth ion site.

The variation in the lifetime was studied as a function of the excitation wavelength. Large changes in the radiative lifetime (more than a factor of three) within the ensemble of Eu^{3+} ions were found to be compatible with the sizable changes observed in the crystal field.

Energy migration studies were only marginally emphasized; observations were limited to those necessary to ascertain the absence of cross-relaxation for these experiments that depend on a single class of sites being excited. It was found that although the onset of cross-relaxation could be observed at very short times after excitation, there was still a detectable line-narrowing signal milliseconds later, indicating a substantial range of energy transfer rates.

Experiments were carried out both at liquid nitrogen and liquid helium temperatures, and it was found that for this system there was little difference in both the characteristics of the line-narrowed spectra and in the rates of energy transfer.

Finally, a set of measurements of linewidths were carried out on the lowest energy component of the $^7F_1$, which undergoes substantial change in position under scanning of the excitation wavelength. The linewidth of this component was observed to change with position above the ground level, (Figure 1) indicating a significant relative contribution of homogeneous broadening to the width. The large density of low frequency vibrations observed for glasses is consistent with the increased homogeneous breadth, as compared with the crystalline case.

The reader is referred to the appendix for the data and a full discussion of these experiments.

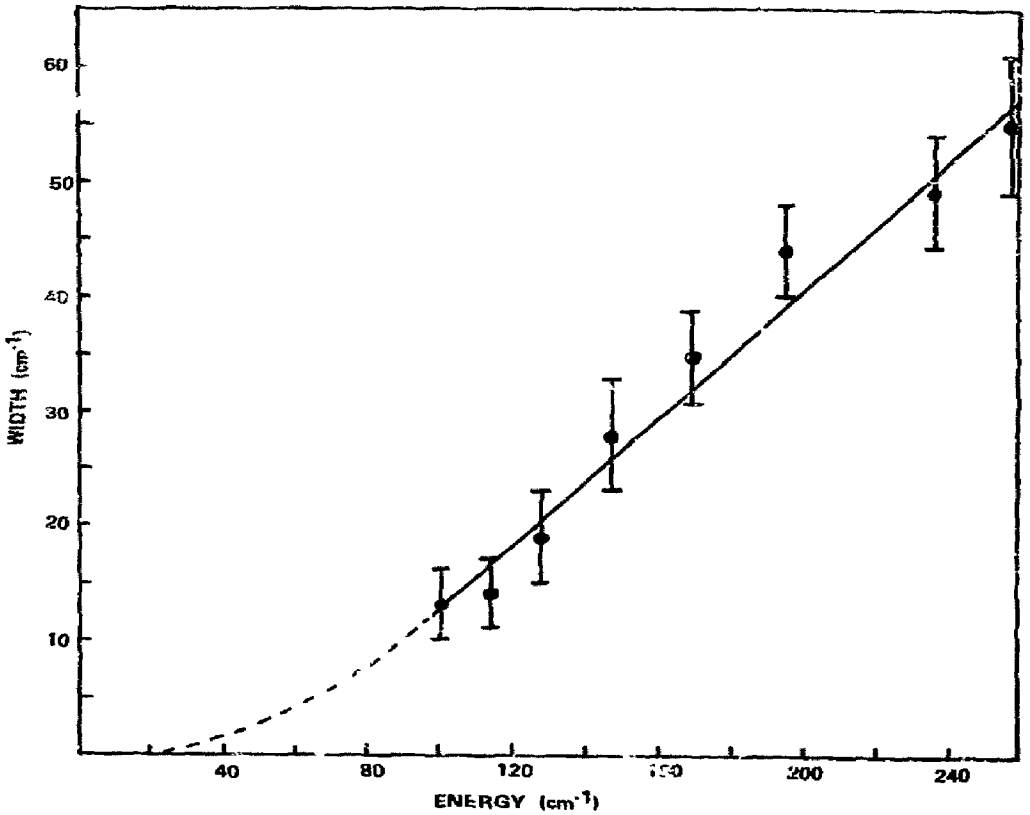

Figure 4. Linewidth of the Shortest Wavelength Component of the $^5D_0 - {}^7F_1$ Transition of Eu^{3+} in L-21 Glass (at 20°K), as Function of the Energy of the Terminal Level

4. OTHER Eu^{3+}-DOPED GLASS SYSTEMS

While most of the effort during the past year centered on the Eu^{3+}-doped sodium barium zinc silicate glass (L-20 and L-21), a number of other systems were also examined. Foremost among these were the twin Eu^{3+}-doped high-lithia phosphate and silicate glasses, L-199 and L-200. Matched in all other respects, these two materials were investigated in an attempt to elucidate the effect of the glass-forming constituent on the environment of the Eu^{3+} ion. Spectra were measured under line-narrowing conditions, at liquid nitrogen temperature, over an excitation range between 5700 and 5850Å; these spectra are shown in Figures 5 and 6. Both materials show behavior similar to that of the L-21 system; in particular, the lowest wavelength component of the $^5D_0$-$^7F_1$ transition shifts widely as the excitation is varied and the shape of the $^5D_0$-$^7F_2$ emission changes markedly.

At equal pump intensities, the emission from the phosphate is considerably more intense than that from the silicate, presumably because of the greater intensity of the $^5D_0$-$^7F_0$ absorption (Figure 7). This enabled measurement of the phosphate emission over the full range of excitation wavelengths, while the silicate emission was too weak at the short and long wavelength extremes. More important, the emission from the phosphate was sufficiently intense to measure the upconversion fluorescence. At all excitation wavelengths above 5810Å, the degree of pumping into the lowest component of the $^7F_1$ state was sufficient to enable a clear resolution of the line-narrowed $^5D_0$-$^7F_0$ emission. The wavelengths of these up-converted lines coincide precisely with the values expected from the normal fluorescence measurements.

Although the spectra of the two materials have not yet been fully processed, it is clear that they are markedly similar. The phosphate does show greater crystal-field splitting than the silicate at the same excitation wavelengths; this, however, is deceptive since the $^5D_0$-$^7F_0$ pump absorption is some 5Å higher in the phosphate. If the excitation is expressed in terms of its relative position with respect to the overall absorption envelope, the crystal-field splittings in the two materials are very nearly the same. This would imply that the ensemble of coordination structures is very similar in the two glasses, but the distribution is not. Again, the detailed crystal-field analysis has not yet been performed.

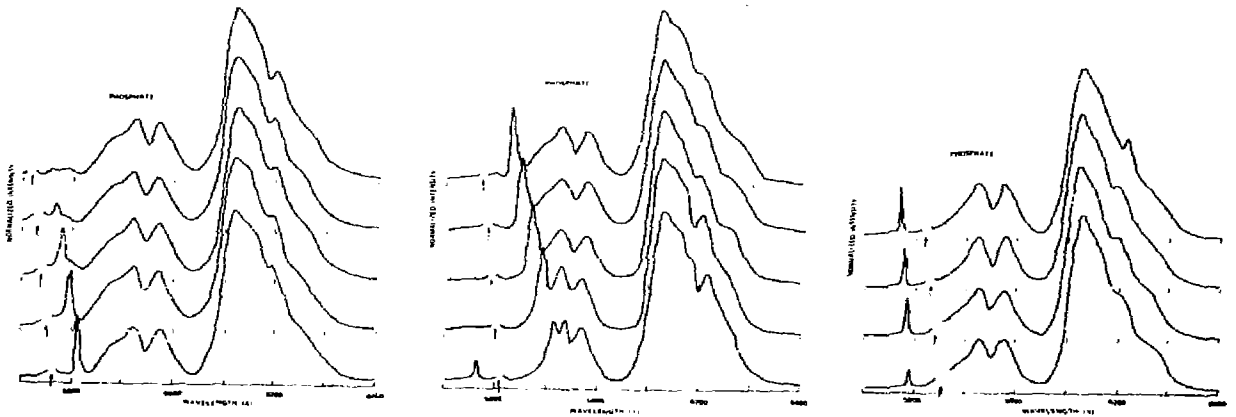

Figure 5. Emission Spectra of Eu^{3+} in L-199 Phosphate Glass (at 80°K) as Function of Excitation Wavelength. Delay time after excitation is 100 μs. Arrows indicate excitation, at 10Å intervals between 5720 and 5850Å. Intensities are normalized with respect to the 6115Å peak at each pump wavelength. Note the "antistokes" $^5D_0 - {}^7F_0$ emission at pump wavelengths above 5800Å.

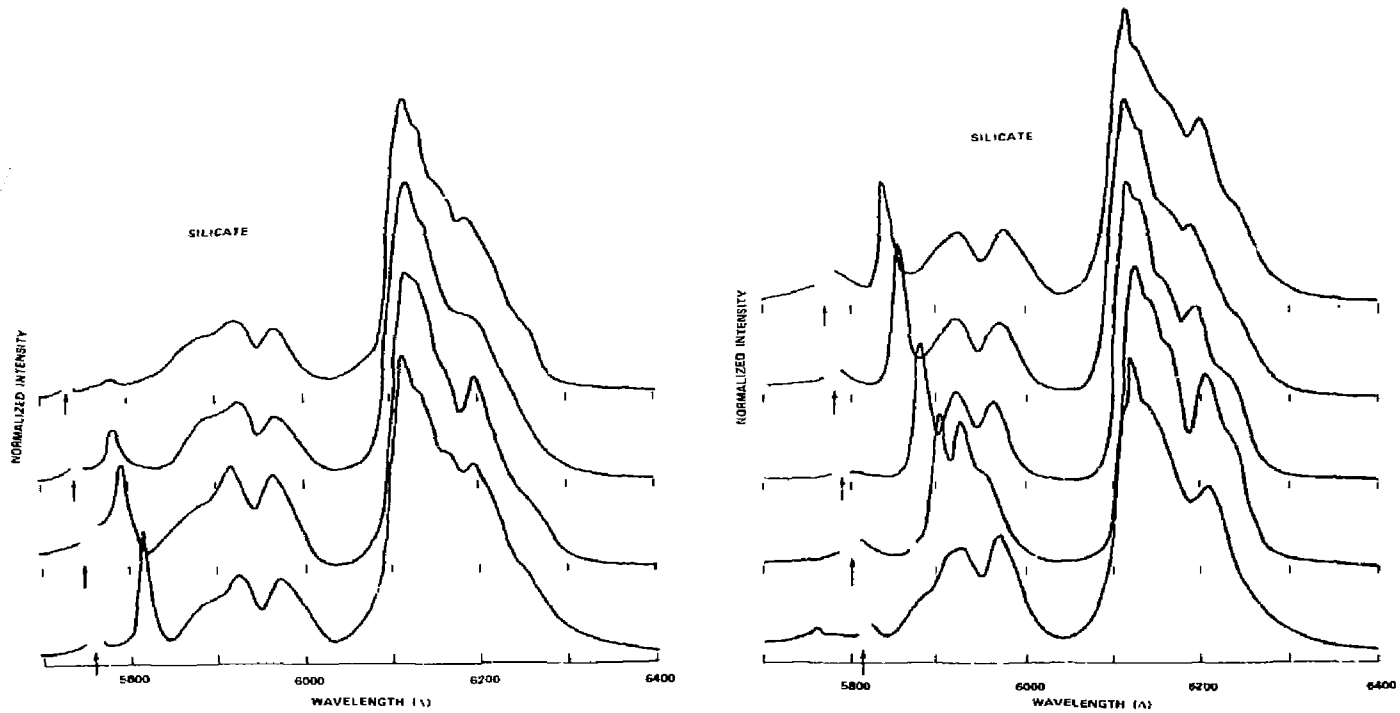

Figure 6. Emission Spectra of Eu^{3+} in L-200 Silicate Glass (at 80°K) as Function of Excitation Wavelength. Delay time after excitation is 100 μs. Arrows indicate excitation at 10Å intervals between 5730 and 5810Å. Intensities are normalized with respect to the 6115Å peak at each pump wavelength. Absolute intensities are much lower than in the phosphate, roughly paralleling the lower absorption intensity of the pump transition.

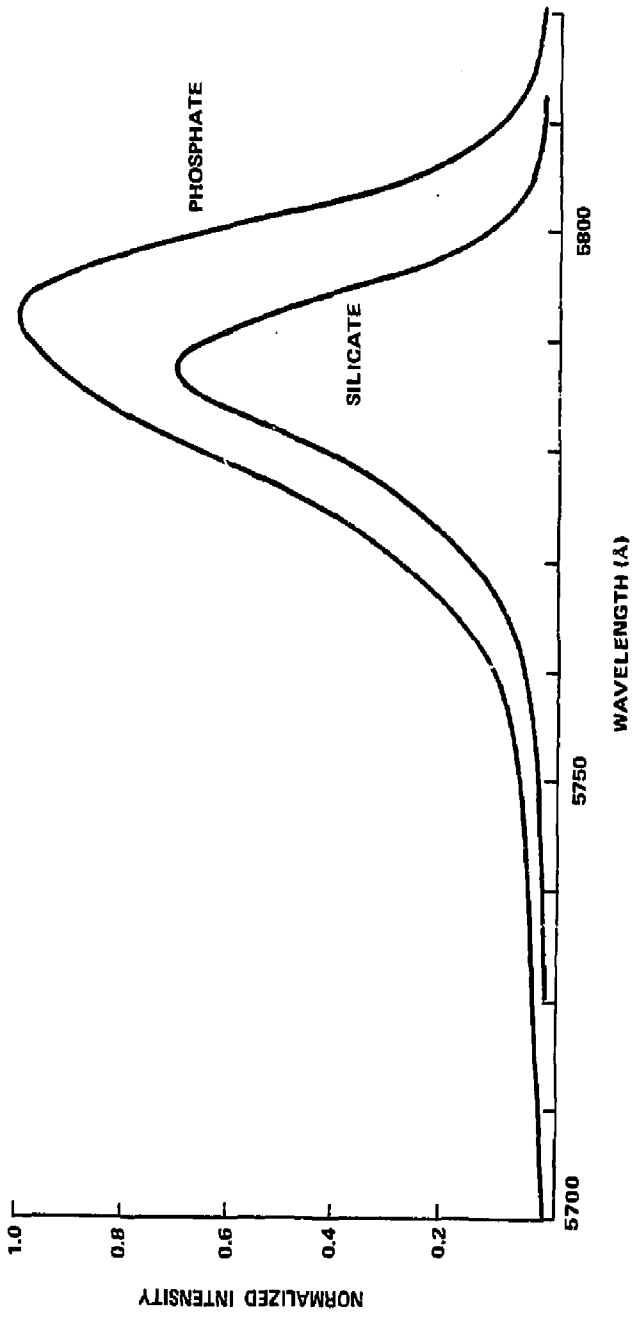

Figure 7. Intensity Profile of the Inhomogeneously Broadened $^5D_0 - {}^7F_0$ Transition of Eu^{3+} in the Phosphate and Silicate Glasses (at 80°K) Used for Excitation

With regard to other glass systems, a Eu^{3+}-doped fused SiO_2 sample was examined briefly and spectral line-narrowing was observed. The specimen was extremely inhomogeneous and was not considered of sufficient quality to process in detail. A $Eu(PO_3)_3$ glass sample was also examined, but at liquid nitrogen temperature the cross-relaxation was too fast for reliable spectra. Liquid helium measurements were planned, but could not be performed during the remaining time. Work on this system must await the appropriate opportunity.

5. CONCLUSIONS AND RECOMMENDATIONS

As a result of the detailed study of the Eu^{3+}-doped barium sodium zinc silicate glass system, a model has been generated for the microscopic structural variation within the range of rare earth ion sites. This work has provided an important step in the rationalization of the spectroscopic properties of rare earth ions in glasses. The next stage of effort should involve a comparative set of such studies in a series of different glasses, for the purpose of extracting the compositional dependence of the spectroscopic properties. Experimental spectra have been generated for high-lithia content phosphate and silicate analogues, and crystal field analyses and structural modeling of these systems should be carried out as the first step in this comparative study.

In view of the specific significance of Nd^{3+}-doped glass systems to the laser fusion program, and the availability of an extensive set of different Nd^{3+}-doped glass samples at LLL, the broad thrust of the compositional variation study should be directed toward the Nd^{3+} glass system. To this end, further experimental work should be based on excitation of isolated levels in the Nd^{3+} ion for the purpose of generating FLN spectra of the $^4F_{3/2} \rightarrow {}^4I_{9/2}$ and $^4F_{3/2} \rightarrow {}^4I_{11/2}$ transitions. Suitable levels for this include the $^2P_{1/2}$ level at approximately 4350Å and the $^4F_{3/2}$ level excited resonantly at 8800Å. The former should be accessible with the N_2 laser pumped dye laser operating with a blue dye. The specific information gathered for the Nd^{3+} system should be independently important in Nd glass laser design, while further probing the spectroscopic effects of compositional variation of glasses.

LASER-INDUCED FLUORESCENCE LINE-NARROWING IN Eu GLASS: A SPECTROSCOPIC ANALYSIS OF COORDINATION STRUCTURE*

by

C. Brecher and L. A. Riseberg

GTE Laboratories, Inc.
Waltham, Massachusetts 02154

*Supported in part by Lawrence Livermore Laboratory

ABSTRACT

By means of the techniques of laser-induced fluorescence line-narrowing, the emission spectrum of Eu^{3+} in a sodium barium zinc silicate glass, and the temporal dependence of the emission, were measured as functions of excitation wavelength. Large variations were observed in the intensities and wavelengths of the various components of the emission. The observed transitions were assigned in terms of a C_{2v} site symmetry, which was found to give an adequate approximation to the symmetry of the local environment of the ion. Crystal field calculations were performed and gave a respectable fit to the observed splittings across the entire range of pump wavelengths. A simple structural model is proposed for the behavior of the first coordination shell of the Eu^{3+} ion in the glassy matrix. The model involves the gradual intrusion of a ninth ligand into an originally octacoordinate site, and is consistent with the signs and relative magnitudes of the experimentally derived crystal field parameters.

APPENDIX

LASER-INDUCED FLUORESCENCE LINE-NARROWING IN Eu GLASS: A SPECTROSCOPIC ANALYSIS OF COORDINATION STRUCTURE

1. INTRODUCTION

A detailed understanding of the optical properties of paramagnetic ions in glasses represents one of the most formidable challenges remaining in solid state spectroscopy. Because an amorphous solid does not have the ordered structure normally found in crystals, the environment of a fluorescent ion is not sufficiently well defined to enable a simple characterization of its optical properties.[1] In the specific case of a rare earth ion in a glass, the spectra are composed of a superposition of contributions from ions distributed among the entire ensemble of local environments. The resulting statistical distribution of Stark components brings about a significant degree of inhomogeneous broadening of the absorption and emission lines and has severely limited the numerous attempts at structural interpretation.[2-6] Similar difficulties have limited the understanding of the excited state kinetics in glassy media.[7-10]

The technique of laser-induced fluorescence line narrowing provides a new and powerful tool for probing the emission properties of ions in disordered systems. This technique, first demonstrated by Szabo[11] and later extended by Riseberg to the case of rare earth ions in glass,[12] involves the selective excitation, within an inhomogeneously broadened absorption line, of a subgroup of ion sites narrowly defined in energy. If the emission can be measured in a time short compared to that necessary for diffusion of energy from the excited ion, the fluorescence observed is specific to that energetically defined subset and is narrowed relative to the inhomogeneous width that is normally observed.

Utilization of time-resolved techniques permits the elucidation of energy transfer processes leading to the redistribution of the excitation throughout the entire population, and a number of such investigations have already been performed.[13-18] In addition, however, observation of the line narrowed spectra permits determination of the energy levels and hence of the crystal field influencing the selected subset. Furthermore, by excitation at various points across the inhomogeneously broadened absorption it becomes possible to map the systematic variations of the crystal field over the entire ensemble of microscopic environments in the glass and to extract information on their structural properties.

In this regard, the unique spectroscopic characteristics of the Eu^{3+} ion make it particularly appropriate for this type of experimental study. The ion has a simple energy level structure and generally well resolved Stark components, thus minimizing

interpretational ambiguities. The emitting state cannot be split by any crystal field, enhancing the precision of site selectivity. And the corresponding inhomogeneously broadened absorption lies at a wavelength ideal for the most powerful dye laser, rhodamine 6G. In this paper we present the results of such a study.

2. EXPERIMENTAL

The material chosen for this investigation was a sodium barium zinc silicate glass doped with Eu^{3+}. The samples, denoted L-20 and L-21, were prepared by the National Bureau of Standards and were provided to us by M. J. Weber of the Lawrence Livermore Laboratory as part of a larger study on fluorescent properties of ions in glasses. The respective percentage compositions are as follows:

L-20(0.09 mol % Eu^{3+}): SiO_2, 74.75; Na_2O, 15.0; BaO, 5.0; ZnO, 5.0; Eu_2O_3, 0.25

L-21(1.10 mol % Eu^{3+}): SiO_2, 72.0; Na_2O, 15.0; BaO, 5.0; ZnO, 5.0; Eu_2O_3, 3.0

Since the only major difference was in Eu^{3+} ion concentration, most of the measurements were performed on the more intensely emitting higher concentration sample, L-21, with just enough attention to the other to ascertain its similarity in behavior. Unless otherwise specified, the subsequent discussion refers only to the higher concentration specimen.

The bulk of the experimental measurements were performed using the techniques of laser-induced line-narrowing spectroscopy. The basic set-up is shown in Figure 1. Excitation was accomplished with a rhodamine 6G dye laser (1×10^{-3} M in ethanol) which in turn was pumped by an Avco Model C 950 pulsed nitrogen laser. The dye cell is wedged to minimize the residual feedback from the cell windows. Tuning was accomplished using a Tropel collimator with anti-reflective optics and a PTR echelle grating. The output could be tuned from 5700Å to 6200Å, and had a typical line width of 2 cm^{-1}. The output pulse had a peak power of approximately 10 Kw, a duration of 15 nanosec, and a repetition rate of 10-20 Hz. The dye laser could also be operated with broadband output extending over the entire inhomogeneously broadened absorption line (Figure 2) by replacing the grating with a mirror.

The excitation was focused on specimens mounted in a Janis Vari-Temp Cryostat, and measurements were made at about 300 K, 80 K and 20 K. The emission was measured with a Jarrell-Ash 1-meter Czerny-Turner monochromator and detected

with an RCA C31034A photomultiplier having an extended S-20 response. A PAR Model 160 Boxcar Averager, triggered by the laser, provided electronically gated signal processing, allowing either fixed or scanned delays. Steady state fluorescence and absorption measurements were also made, using routine techniques. Spectra were measured with the laser tuned at 10 Å intervals between 5730 Å and 5810 Å; these are shown in Figure 3, and the pertinent wavelengths are listed in Table 1. The line-narrowing effect is immediately evident, the most striking feature being the strong shift in the lowest component of the $^5D_0 - {}^7F_1$ emission, especially when compared with the emission under broad band laser or steady state lamp excitation (Figure 4). This component is much sharper than the others, but some sharpening and shifts are measured in all. Similar shifts are observed in the $^5D_0 - {}^7F_2$ emission region, which shows dramatic changes in overall shape. The $^5D_0 - {}^7F_3$ and $^5D_0 - {}^7F_4$ regions have been sampled, but because of incomplete resolution are not useful in the subsequent interpretation.

3. DISCUSSION

A. Site Selectivity and Energy Migration

Although the line-narrowing effect is readily observable in the measured spectra, the validity of the interpretation depends rather significantly on the degree of site selectivity that this in fact represents. This site selectivity can be degraded in a number of ways. Simplest among these is non-monochromaticity of the exciting radiation. The rhodamine 6G dye laser has such a high intrinsic gain that it is impossible to suppress entirely the untuned broadband emission caused by super-radiance and stray non-selective feedback. The peak intensity of this emission is some three orders of magnitude below that of the tuned line of the laser; since its bandwidth is a factor of 100 greater, however, it can contribute significantly to the total exciting radiation falling on the sample. The contribution can be ascertained by blocking the feedback from the grating and measuring the residual fluorescence from the sample. The contribution is not important except at the extremes of the pump wavelength range, where it can be as much as 20% of the line-narrowed signal.

Another cause of degradation of the site selectivity is energy migration. This effect is demonstrated in Figure 3, which shows the deterioration of the line-narrowing effect as the delay time of the measurement is increased from 50 microsec to 5 millisec. Note that the respective spectra change toward that measured under broad band

excitation (Figure 4), of which the shoulder at about 5880Å is the most readily distinguishable feature. The fact that the latter is observed only 50 microsec after excitation even at 20 K, while some line narrowing persists 5 millisec later (and even at 300 K in the more dilute sample) indicates a remarkably broad range of cross-relaxation times. We do not choose to consider this question in detail; suffice it to say that the incremental degradation of the line narrowed signal is small, and that at times short compared to the fluorescence decay (as in most of our measurements) the line narrowed spectrum constitutes the bulk of the contribution.

A final question concerns the remaining degree of inhomogeneity in the measured spectra. In the subsequent discussion it is assumed that the energy of that $^5D_0$ state pertinent to a particular spectrum is defined by the energy of the pump line, and that conversely the rest of the spectrum is characteristic of the single class of sites selected. Although it is conceivable that two or more sites differing widely in their crystal field properties may have the same $^5D_0 - {}^7F_0$ energy, we observe no line narrowed components whose interpretation requires a second site. The homogeneous widths should be large,[10] however, as expected from the high density of low energy phonons in glass; any residual inhomogeneous contribution (as reported in the $Ca(PO_3)_2$ glass system[16]) would be considered unimportant as long as it does not change the measured position of the component.

B. *Assignment and Interpretation*

The disordered nature of the glassy matrix presents a major impediment to the interpretation of the spectra. The lack of anything higher than trivial (C_1) symmetry removes all selection rules, allowing all transitions to appear in all directions; furthermore, the lack of long range correlation between sites prevents the use of polarization behavior as a criterion for establishing the identity of a given transition. Nevertheless, certain features common to the entire set of spectra indicate that some degree of local order persists in the immediate environment of the emitting ion. We observe, for example, that although the emission from the $^5D_0$ level to be $^7F_1$ and $^7F_2$ states are split into the maximum number of components (3 and 5, respectively), these components differ markedly in their behavior. In the $^7F_1$ region, for example, the shortest wavelength component is considerably sharper than the other two and its location is much more sensitive to the pump wavelength. In the $^7F_2$ region, the lower three components are substantially more intense than the other two and shift less in energy. And finally there is a clear systematic correspondence between the respective spectral components at different excitation wavelengths.

In view of these points, we feel it appropriate to assign the spectra in terms of an "almost symmetry", in which the immediate environment of the ion is assumed to possess an average local order not found in the bulk, and that the lowering of symmetry below this level reflects largely the randomness of orientation from one site to the next. For this treatment the most appropriate symmetry is C_{2v}: It is the highest symmetry in which full splitting of the $^7F_1$ and $^7F_2$ levels is allowed while maintaining symmetry-based distinctions between almost all the components. This point group allows optical activity for the three $^5D_0 - {}^7F_1$ components and for four of the five $^5D_0 - {}^7F_2$ components. It is a subgroup of almost all of the higher point symmetries in which rare earth ions are normally found, enabling application of the standard technique of descending symmetries. And finally, it is the lowest symmetry for which simple crystal field calculations can be routinely performed. The importance of this last point will become evident below.

As a starting point, the unique behavior of the shortest wavelength component of the $^5D_0 - {}^7F_1$ transition assumes considerable importance. This component, much sharper than the others and shifting more than 100 Å as a function of pump wavelength, is assigned to the transition terminating in the $M_J = 0$ level of the $^7F_1$. This level is non-degenerate in all axial symmetries higher than C_1 and does not mix with any of the other levels until all axial symmetry is removed. In C_{2v} the level belongs to the A_1 representation; the other two therefore belong to the B_1 and B_2 representations, although the ordering remains ambiguous.

In the $^7F_2$ region we observe that the three shorter wavelength components are consistently more intense and shift less in wavelength than the other two. By the descending symmetries argument,[17] we take this to be indicative of some residual higher axial symmetry. Following the point group correlations (Table 2), the best set of assignments identifies the terminal level of the three shorter wavelength components as A_1, B_1, B_2, while the other two fall into A_1 and A_2. Again the ordering is ambiguous.

In order to choose among the 24 combinations of assignments consistent with the above argument, we apply elementary crystal field calculations. In view of the limitations of such calculations and the approximations already made, it would be difficult to justify this approach for any single set of energies. In this case, however, we do not have merely nine unrelated spectra, but rather a basic continuity, in which the overall intensity relationships are maintained and the location and shape of

individual components can be followed as continuous functions of the pump wavelength. We therefore must disregard best fits that require discontinuous changes in assignment as the pump wavelength is scanned, and instead seek a best assignment common to the entire set. We also disregard assignments for which the fit is substantially better at one end of the pump wavelength range than at the other. Applying these additional criteria we find only two sets of assignments that are at all acceptable; the better of these, with the observed and calculated energies, is listed in Table 3. The pertinent crystal field parameters are listed in Table 4.

In order to generate a geometric model for the structure of the immediate environment of the emitting ion, a number of additional assumptions are necessary. Since the number of ligands is unspecified, we assume as a starting point that, in the the absence of lattice-imposed constraints to the contrary, the bulk of the Eu^{3+} ions reside in sites of eight-fold coordination. With few exceptions such behavior is characteristic of Eu^{3+} in oxide-type media and is consistent with considerations of relative ionic size (0.7:1) and number of available bonding orbitals (9). We treat the eight immediate ligands as if they were equidistant from the central ion and disregard as insignificant the contributions to the crystal field of any other neighboring ligands lying at more than twice the primary distance.[18]

Next we observe that the most efficient packing of eight unit spheres around a central sphere of radius roughly 2/3 is the square Archimedean antiprism, symmetry D_{4d} (Figure 6a). Taking this uniaxial arrangement as the parent structure for a descending symmetries treatment, we perform a continuous and gradual distortion, systematically removing symmetry elements to reach the desired lower biaxial symmetry of C_{2v}.[19]

The nature and magnitude of this distortion can be extracted from the derived crystal field parameters, each of which can be expressed as the product of two factors: the relevant tesseral harmonics (which contains the bulk of the orientational information); and a scaling factor involving charge magnitude, coordination distance, and radial expectation values for the 4f electrons. We choose to disregard the latter factor, and extract the pure orientational information by considering ratios of the parameters of the same order; e.g., B_{22}/B_{20}, B_{44}/B_{40}. These values can be calculated for any appropriate geometrical arrangement of eight ligands; however, when compared with the corresponding experimentally determined values, reasonable agreement can be achieved only at the long excitation wavelength limit of the set. The corresponding

structure is shown in Figure 6b. For successively shorter excitation wavelengths the disagreement rapidly becomes intolerable; indeed, we are unable by any systematic distortion to generate a reasonably close-packed eightfold coordination structure whose calculated crystal field parameters behave in the appropriate manner. To resolve this inconsistency, we direct our attention to the massive changes in the mean energies of the various spin-orbit states. For example, the barycenters of the $^7F_1$ and $^7F_2$ states shift in energy by more than 25% over the range of excitation wavelengths. Such shifts, although clearly beyond the realm of elementary electrostatic crystal field theory (which deals only with splittings from the barycenters and does not cover finer interactions, such as J-mixing), clearly implies a substantial and systematic increase in the total external field influencing the ions excited at the shorter wavelengths. This is consistent with the parallel decrease observed in the radiative lifetimes at the shorter wavelengths (see lifetime section following). Even more significant is the total breadth of the $^5D_0$ state, which, as seen from the absorption profile (Figure 2) spans an energy range of some 300 cm^{-1}. In other host systems, where shifts one-tenth this amount are considered large, such shifts have always been associated with changes in the chemical nature of the environment; that is, in the number or the bonding properties of the coordinating ligands.[20] The disordered nature of the glassy host gives all the more reason to expect similar effects in the case at hand.

We propose, therefore, to treat the set of spectra in terms of a systematic decrease in the average distance of a ninth coordinating ligand. We consider this the most appropriate treatment for a number of reasons:

1. The relative ionic radii are appropriate ($r_{Eu^{3+}} : r_{O^{2-}} = 0.7:1$). Close-packed nine-fold coordination requires only a 2-3% increase in the mean radial distance to equivalent coordinators over that required for the corresponding close-packed eightfold coordinated structure.

2. The medium is dilute in terms of Eu^{3+} (appr. 1 mol%) and thus oxygen-rich in terms of ligands available for coordination. The Eu^{3+} ion has sufficient empty orbitals available for bonding (sp^3d^5) and will accept the maximum coordination allowed within the constraints of the glassy network.

3. The requisite gradual coordination change can take place within the context of an overall C_{2v} local symmetry. This gives a geometrical rationalization for the observed consistency in intensity patterns and continuity in component identification despite the rather large shifts in energy.

We therefore generate the following model for the average structure of the Eu^{3+} sites in the glassy host: Beginning with eight approximately equidistant oxygens in a geometric arrangement of a slightly elongated Archimedean antiprism we allow a ninth oxygen to approach along the two-fold symmetry axis. The other eight shift their position to accommodate the interloper, until at the completion of the process all nine are approximately equidistant from the Eu^{3+} ion. The process is a continuous one, and can be described through a distortion parameter ϵ, having limiting values of zero (pure eight-fold coordination) and unity (fully transformed to nine-fold, equidistant coordination). Two stages are shown in Figure 6c and d.

Crystal field parameters can be calculated for the various geometrical arrangements associated with the respective values of the distortion parameter ϵ. As shown in Table 5 and Figure 7, the agreement with the experimentally determined values is remarkably good. All the parameters increase or decrease in the appropriate manner as a function of ϵ, and all have the appropriate signs throughout. One, the B_{42} parameter, is considerably smaller in magnitude than the measured value; this parameter, however, is the least precise of the set, entering only in the exchange terms in the calculations for the experimental fit. The B_{44} value does, in fact, change sign as predicted. The best agreement is in the major ratios (Figure 8): As ϵ increases from 0 to 1, B_{22}/B_{20} decreases by a factor of eight and B_{44}/B_{40} increases more than 15- fold, changing sign in the process. The values agree sufficiently well to enable a correlation between pump wavelength and distortion parameter (Figure 9). An even better agreement could be obtained if we were to remove some of our self-imposed limitations from the model, such as equidistance for the eight primary coordinators, but such further refinement would not be useful. The agreement is most respectable as it stands, and we feel that the simple model described gives a reasonable approximation for the site variation behavior in this glassy medium.

C. Decay Times

In an attempt to shed additional light on the nature of the multiple sites in the glass, measurements were made of the fluorescence decay as a function of pump

wavelength. If the sites selectively excited by the pump light are as distinct as indicated by the spectra, the structural differences should be reflected in characteristic differences in the fluorescence decay time. This is indeed the case, with the apparent decay times becoming increasingly shorter as the wavelength of the pump is decreased. The picture revealed by these measurements is, however, somewhat clouded; in all cases, at both liquid nitrogen and liquid helium temperatures, the decay curves are distinctly non-exponential. This is clearly to be expected, in view of the spectroscopic evidence (discussed earlier) that a significant degree of non-line-narrowed emission underlies all the ostensibly line-narrowed spectral components. In order to extract the information relevant to the particular site in question, further processing is required.

One approach is simply to accept the non-exponential behavior and to fit the resultant curved plot of log I vs. time by including a quadratic term:

$$\log I = \log I_0 - \alpha t + \beta t^2$$

As long as the linear coefficient α remains relatively large compared to βt (short time limit), we can extract the value of the faster lifetime $\tau = 1/\alpha$ with a reasonable degree of confidence.

A better approach, in principle, would be to correct for the underlying (long-lived) background. The line-narrowed spectral components, although generally broader than would be desired, are still considerably sharper than those excited under non-line-narrowing conditions (broadband pulse or continuous). We therefore approximate the decay curve of the non-line-narrowed contribution underlying the component in question by the arithmetic mean of decay curves measured 20 Å on either side of the peak; this is then subtracted from the corresponding measurements at the peak wavelength, yielding a decay curve that arises essentially from the line-narrowed component alone. Of the eight spectral components only two --- the highest and lowest members of the $^5D_0 - {}^7F_1$ set --- are sufficiently well resolved throughout the range of pump excitation to justify this treatment. The decay values derived from this approach, however, agree to within 10% with those obtained from the first approach, and are not reported separately.

The decay times of the $^5D_0$ state were determined at all pump wavelengths of interest, and are summarized in Table 6 and Figure 10. Measurements were made at the wavelengths of the various line-narrowed components of the emission; these

should of course be redundant, the overall lifetime of the $^5D_0$ state being independent of the particular transition measured. In fact, however, a systematic discrepancy is observed between the lifetime values derived from the shortest wavelength component of the line-narrowed $^5D_0 - {}^7F_1$ transition and the values derived from the others. This component consistently exhibits a shorter lifetime, and the discrepancy increases as the pump wavelength is decreased. We attribute the discrepancy to the uniquely high spectral resolution of the component, superimposing the strongest and sharpest line-narrowed contribution upon the most diffuse non-line-narrowed background. Since the long-lived background (≈2.2 msec) would tend to distort the line-narrowed measurements toward higher values (with greater distortion for shorter lifetime value), and the treatment depends on our ability to separate this contribution, we accept the lower values as the true measure of the decay times of the $^5D_0$ state.

The most significant point about the decay times is their systematic behavior as a function of pump wavelength. The decay time is a maximum at a pump wavelength of 5800 Å, decreasing gradually and monotonically to less than 1/3 of this value at the short wavelength limit of the pump. A corresponding but precipitous drop occurs toward the long wavelength pump limit, the decay time decreasing by at least a factor of four in only 10 Å. These measured values presumably correspond to the radiative lifetimes since the total emission intensity at any given pump wavelength is very nearly proportional to the absorbed pump energy, as determined from the absorption constant and the laser beam intensity.

To explain the behavior of the lifetimes at pump wavelengths 5800 Å and below is quite straightforward. The progressive increase in the corresponding radiative transition probabilities parallels the apparent increase in the total crystal field, particularly that of the second order term B_{20}. In addition, it is quite consistent with the geometric model previously described, which postulates an increase in the number of ligands in the first coordination sphere. The accompanying rearrangements also increase the magnitude of the odd terms in the crystal field (particularly B_{30}, B_{32} and B_{50}, which show increases greater than a factor of four), implying a consequent increase in the electric dipole transition possibilities. We consider this predicted increase to be supportive of the model.

The lifetime behavior at pump wavelengths longer than 5800 Å is more difficult to understand. Presumably the radiative lifetime should continue to increase as the magnitude of the total crystal field decreases. Note, however, that at the shorter

pump wavelengths (the high-field sites) the emission corresponding to the lowest $^5D_0$ - $^7F_1$ component has shifted below the long wavelength limit of the $^5D_0$ - $^7F_0$ pump line. Furthermore, the energy of the lowest Stark component of the $^7F_1$ state in the high-field sites is little more than 100 cm^{-1} above ground, so that even at liquid nitrogen temperature that level contains some 10-15% of the total population of those sites. Thus as the absorption due to the direct $^5D_0$ - $^7F_0$ transition in low-field sites drops off above 5800 Å, the absorption at the same wavelength due to the $^5D_0$ - $^7F_1$ transition in high field sites may become dominant. The measured lifetime should then decrease to values characteristic of the latter sites. This is supported by the observation of an anti-Stokes line-narrowed $^5D_0$ - $^7F_0$ emission at the appropriate wavelengths corresponding to the high field sites excited by the $^5D_0$ - $^7F_1$ absorptions. The persistence of the effect, at a diminished level, even near liquid helium temperature indicates that some unspecified energy transfer process may also be a contributing factor. As indicated earlier, the question of energy migration is complex, and will be treated elsewhere[14, 15] but the lifetime behavior presents no major inconsistencies with the structural interpretation.

4. CONCLUSION

The spectroscopy of Eu^{3+} in glass has been partially clarified by applying the techniques of laser-induced line-narrowing to the inhomogeneously broadened emission. The components of the emission, excited at various pump wavelengths, have been assigned and their decay times measured. From these measurements the corresponding energy levels within the $^7F_1$ and $^7F_2$ multiplets were ascertained and the functional dependence of the crystal field was calculated over the range of sites selected by the pump wavelengths.

To provide a physical rationalization for the behavior of the crystal field parameters, a geometric model was generated. This model involves a gradual change from eight-fold to nine-fold coordination in the immediate environment of the Eu^{3+} ion, while maintaining an overall C_{2v} symmetry throughout. The model predicts crystal field parameters whose behavior agrees well with the experimentally derived values, and we feel that it gives a reasonable approximation to the average structure of the emitting site.

ACKNOWLEDGEMENT

The authors wish to express their gratitude to M. J. Weber for many helpful discussions and his deep interest in and support of this work. We thank W. M. Yen, J. A. Faisner and H. Samelson for their useful advice and suggestions, and B. W. Hawkins and J. Walsh for their expert technical assistance.

REFERENCES

1. J.A. Prins, in "Physics of Non-Crystalline Solids", edited by J.A. Prins (John Wiley and Sons, Inc., N.Y. 1965) p. 1.

2. D.k. Rice and L.G. DeShazer, Phys. Rev. 186, 387 (1969).

3. M.M. Mann and L.G. DeShazer, J. Appl. Phys. 41, 2951 (1970).

4. C.C. Robinson and J.T. Fournier, Chem. Phys. Letters 3, 517 (1969), J. Phys. Chem Solids 31, 895 (1970).

5. J.T. Fournier and R.H. Bartran, J. Phys. Chem. Solids 31, 2615 (1970).

6. C.C. Robinson, J. Chem. Phys. 54, 3572 (1971).

7. L.G. DeShazer, in "Optical Properties of Ions in Crystals", edited by H.M. Crosswhite and H.W. Moos (Interscience Publishers, Inc., New York, 1967). p. 507.

8. M.J. Weber, E.J. Sharp, and J.E. Miller, J. Phys. Chem. Solids 32, 2275 (1971); M.J. Weber, Phys. Rev. B4, 2932 (1971).

9. L.A. Riseberg and M.J. Weber, in "Progress in Optics", edited by E. Wolf (North Holland Publishing Co, Amsterdam, 1975), Vol. 14, and references cited therein.

10. Yu V. Denisov, I.V. Kovaleva, V.P. Kolobkov, and V.V. Rastoskuev, Opt. Spectrosc. 38, 54 (1975).

11. A. Szabo, Phys. Rev. Letters 25, 924 (1970); ibid. 27, 323 (1971).

12. L.A. Riseberg, Phys. Rev. Letters 28, 789 (1972); Solid State Communications 11, 469 (1972); Phys. Rev. A7, 671 (1973).

13. N. Motegi and S. Shionoya, J. Luminescence 8, 1 (1973).

14. W.M. Yen, S.S. Sussman, J.A. Paisner, and M.J. Weber, Bull. Am. Phys. Soc. 20, 44 (1975).

15. J.A. Paisner, S.S. Sussman, W.M. Yen, and M.J. Weber, Bull. Am. Phys. Soc. 20, 447 (1975).

16. T. Kushida and E. Takushi, (to be published).

17. B.G. Wybourne, "Spectroscopic Properties of Rare Earths" (Interscience Publishers, New York, 1958) p. 708.

18. M.T. Hutchings and D.K. Ray, Proc. Phys. Soc. (London) 81, 663 (1963).

19. See, for example, C. Brecher, J. Chem. Phys. 61, 2297 (1974).

20. H. Samelson, C. Brecher, and A. Lempicki, J. Molec. Spectry., 19, 349 (1966).

FIGURE CAPTIONS

Figure 1. Experimental apparatus for laser-induced fluorescence line-narrowing measurements.

Figure 2. Intensity profile of the inhomogeneously broadened $^5D_0 - {}^7F_0$ resonance transition of Eu^{3+} in L-21 glass (at 80 K) used for excitation.

Figure 3. Emission spectra of Eu^{3+} in L-21 glass (at 20 K) as function of excitation wavelength. Arrows indicate excitation, at 10Å intervals between 5730 and 5810Å. Delay time after excitation pulse, 100 μsec. Intensities normalized to 6113Å peak at each pump wavelength; for approximate comparison of intensities at different pump wavelengths, multiply by the respective intensities of the pump transition, Figure 2.

Figure 4. Emission spectra of Eu^{3+} in L-21 glass (at 80 K) under broadband excitation. Upper spectrum, continuous excitation in 3900Å region; lower spectrum, *pulsed excitation by free-running (untuned) dye laser emitting in* broadband over full range of $^5D_0 - {}^7F_0$ absorption (indicated by arrows).

Figure 5. Emission spectra of Eu^{3+} in L-21 glass (at 80 K) as function of delay time after excitation pulse. (a) Excitation at 5770Å; (b) excitation at 5800Å. Upper spectrum in each case measured at 50 μsec. delay, lower spectrum at 5 millisec delay.

Figure 6. Geometric models for the environment of the Eu^{3+} ion in L-21 glass. The Eu^{3+} ion is depicted at the origin, and the eight equiradial coordinating oxygens are shown as located at the vertices of the solid geometric figure defined by connecting their centers. The structures are drawn in perspective as viewed approximately from the (111) direction, with the coordinate axes shown where they emerge from the solid figure. The square Archimedean antiprism is shown in (a), with points A, B, C, D and E, F, G, H forming two squares perpendicular to the z-axis. The best-fitting pure eight-fold structure is shown in (b), which is derived from (a) mostly by motion of points F and H in the -z direction. The structure remains essentially unchanged by the approach of the ninth coordinator I along the z-axis, until its radial distance decreases to 1.4 times that of the other eight coordinators. Closer approach requires a spatial rearrangement of the latter, which can be expressed in terms of a parameter ϵ, the fraction of the remaining decrease in distance needed to achieve equiradial nine-fold coordination. Structures (c) and (d) correspond to ϵ values of 0.1 and 0.9, respectively. Note the major distortions: ABCD becomes longer and rectangular (AB = 1.05 × AD), and points E and G move beyond points F and H in the -z direction.

Figure 7. Behavior of the crystal field parameters B_{20}, B_{22}, B_{40}, B_{42}, and B_{44} as functions of pump wavelength and distortion parameter. Symbol • indicates experimental measurement, o indicates calculation from geometric model. Values normalized with respect to maximum value in each case. Note that in all cases there is a monotonic relationship between distortion parameter and wavelength, and that both measured and calculated values span roughly the same range.

Figure 8. Behavior of the major crystal field ratios B_{22}/B_{20} and B_{44}/B_{40}. Symbol • indicates experimental measurement, symbol o indicates calculation from geometric model. Unlike Figure 7, these are ratios of the actual values of the respective parameters, and carry the full geometric information. Note the substantial agreement except at the most extreme cases; only the described model gives agreement over such a wide range.

Figure 9. Relation between pump wavelength and distortion parameter ϵ. Values extracted by interpolation along curves in Figure 8. Note the roughly sigmoid approach to nine-fold coordination.

Figure 10. Decay time of fluorescence of Eu^{3+} in L-21 glass (at 20°K) as function of pump wavelength. Symbol • indicates measurements of longest wavelength component of $^5D_0 - {}^7F_1$ transition; symbol o, shortest wavelength component. While the discrepancy indicates a residue of unresolved longer-lived non-line-narrowed contribution in the former case, the parallel decrease with pump wavelength confirms that the major contribution is indeed the line-narrowed emission.

TABLE I

EMISSION WAVELENGTHS OF Eu^{3+} IN L-21 GLASS AS FUNCTIONS OF PUMP WAVELENGTH

PUMP WAVELENGTH (Å)	EMISSION WAVELENGTHS (Å)							
5810	5911	5925	5959	6101	6113	6169	6199	6244
5800	5888	5925	5965	6100	6113	6162	6198	6256
5790	5867	5926	5971	6099	6113	6157	6197	6266
5780	5846	5926	5975	6098	6113	6153	6197	6274
5770	5827	5925	5976	6097	6112	6151	6198	6277
5760	5810	5924	5974	6096	6112	6150	6199	6273
5750	5793	5923	5970	6095	6111	6150	6190	6267
5740	5778	5922	5966	6054	6111	6150	6199	6260
5730	5764	5920	5962	6092	6110	6149	6197	6252

TABLE II

CORRELATION MAPPINGS AND SELECTION RULES FOR THE RELEVANT SYMMETRIES

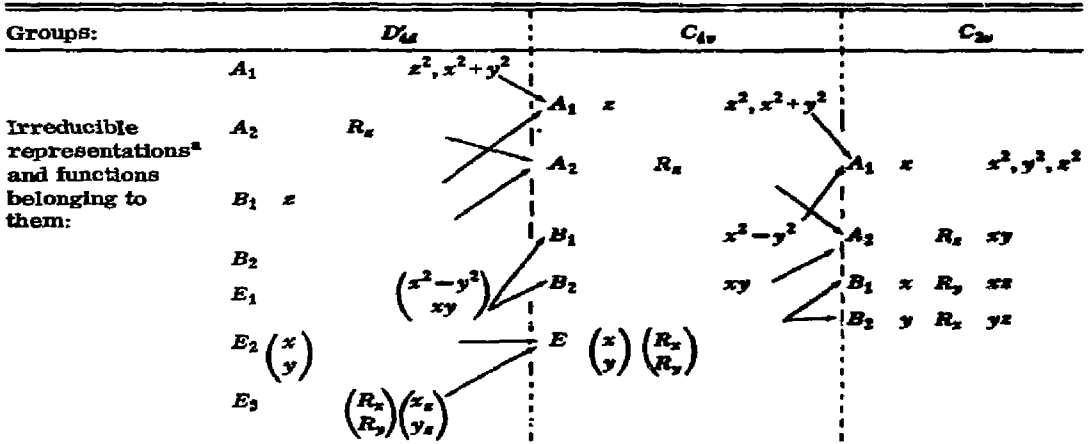

Transitions	Representations[b] to which transitions belong		
0—0	A_1	$\underline{A_1}$	$\underline{A_1}$
0—1	$\underline{A_2}+\underline{E_2}$	$\underline{A_2}+\underline{E}$	$\underline{A_2}+\underline{B_1}+\underline{B_2}$
0—2	$A_1+E_1+E_3$	$\underline{A_1}+B_1+B_2+\underline{E}$	$\underline{2A_1}+A_2+\underline{B_1}+\underline{B_2}$

[a]Because of nonstandard orientations of the coordinate axes, the representations for group D_{4d} differ from those usually found. The coordinate axes are contained in reflection planes *rather than rotations*, so as to facilitate correlation to C_{4v}.

[b]Representations underlined are those for which optical activity is allowed; magnetic dipole for the 0-1 transition, electric dipole elsewhere.

TABLE III

ENERGY LEVELS OF Eu^{3+} IN L-21 GLASS AS FUNCTIONS OF PUMP WAVELENGTH ASSIGNMENT (IN TERMS OF C_{2v} SYMMETRY)

PUMP WAVELENGTH		$^7F_1$			$^7F_2$				
		A_2	B_1	B_2	A_1	A_1	A_2	B_1	B_2
5810	observed	294	334	430	853	1196	1080	821	1002
	calculated	295.3	326.0	436.1	869.2	1177.0	1083.4	802.9	1015.9
5800	observed	258	364	477	883	1257	1107	848	1013
	calculated	257.3	354.3	487.7	904.6	1230.1	1105.3	825.8	1037.3
5790	observed	227	396	524	913	1312	1134	875	1029
	calculated	224.2	388.3	535.9	934.3	1284.6	1126.4	857.5	1056.0
5780	observed	195	426	565	942	1362	1164	902	1049
	calculated	191.4	421.3	575.2	960.5	1338.9	1154.1	891.3	1072.1
5770	observed	170	453	597	970	1400	1197	930	1074
	calculated	166.9	450.6	604.0	983.9	1383.8	1188.6	924.5	1090.0
5760	observed	149	481	622	1000	1420	1229	957	1101
	calculated	147.9	480.5	624.1	1004.0	1415.0	1226.1	955.8	1105.8
5750	observed	129	508	641	1027	1435	1260	984	1131
	calculated	130.6	508.4	638.2	1021.5	1441.9	1264.3	985.0	1124.6
5740	observed	115	535	660	1058	1447	1290	1012	1161
	calculated	119.9	535.6	652.1	1041.9	1467.1	1303.4	1013.3	1143.0
5730	observed	103	560	679	1085	1457	1315	1037	1189
	calculated	111.5	560.1	666.1	1058.1	1490.6	1338.2	1037.2	1159.8

TABLE IV

CALCULATED CRYSTAL FIELD PARAMETERS FOR Eu^{3+} IN L-21 GLASS

PUMP WAVELENGTH	CRYSTAL FIELD PARAMETERS (cm^{-1})						
	$\bar{E}_1$	$\bar{E}_2$	B_{20}	B_{22}	B_{40}	B_{42}	B_{44}
5810	352.5	989.5	-143.0	275.2	-128.2	1065.9	375.5
5800	366.4	1020.6	-272.7	333.7	-119.0	1108.1	97.6
5790	382.8	1051.9	-396.4	368.9	-105.6	1085.9	-172.7
5780	395.9	1083.4	-511.4	384.7	- 94.7	1029.4	-381.7
5770	407.2	1114.0	-600.7	383.6	- 86.2	968.0	-489.6
5760	417.5	1141.4	-674.0	359.1	- 78.6	886.8	-523.4
5750	425.7	1167.4	-737.9	324.5	- 69.6	817.8	-524.3
5740	435.9	1193.7	-789.8	291.3	- 64.7	750.9	-504.4
5730	445.9	1216.8	-836.0	265.1	- 60.5	701.4	-483.6

TABLE V

CRYSTAL FIELD RATIOS FOR VARIOUS STRUCTURES AND PUMP WAVELENGTHS

DISTORTION PARAMETER (ϵ)	PUMP WAVELENGTH (Å)	B_{22}/B_{20}	B_{44}/B_{40}
0		-2.05	-0.61
	5810	-1.92	-0.93
0.1		1.27	-0.12
	5800	-1.22	-0.82
0.3		-1.00	+0.83
	5790	-0.93	1.64
0.5		-0.91	1.63
0.7		-0.83	2.59
	5780	-0.75	4.03
0.8		-0.75	3.71
	5770	-0.64	5.68
0.9		-0.54	6.45
	5760	-0.53	6.66
	5750	-0.44	7.53
	5740	-0.37	7.80
	5730	-0.32	7.99
1.0		-0.23	9.56

TABLE VI

DECAY TIMES OF Eu^{3+} FLUORESCENCE IN L-21 GLASS

PUMP WAVELENGTH (Å)	DECAY TIME (MILLISEC) LOWEST $^7F_1$ COMPONENT	DECAY TIME (MILLISEC) HIGHEST $^7F_1$ COMPONENT
5810	0.64	0.59
5808	1.09	1.12
5805	1.88	1.84
5800	2.18	2.18
5790	1.95	2.12
5780	1.56	1.98
5770	1.21	1.79
5760	0.94	1.42
5750	0.77	1.15
5740	0.62	0.88
5730	0.45	0.79

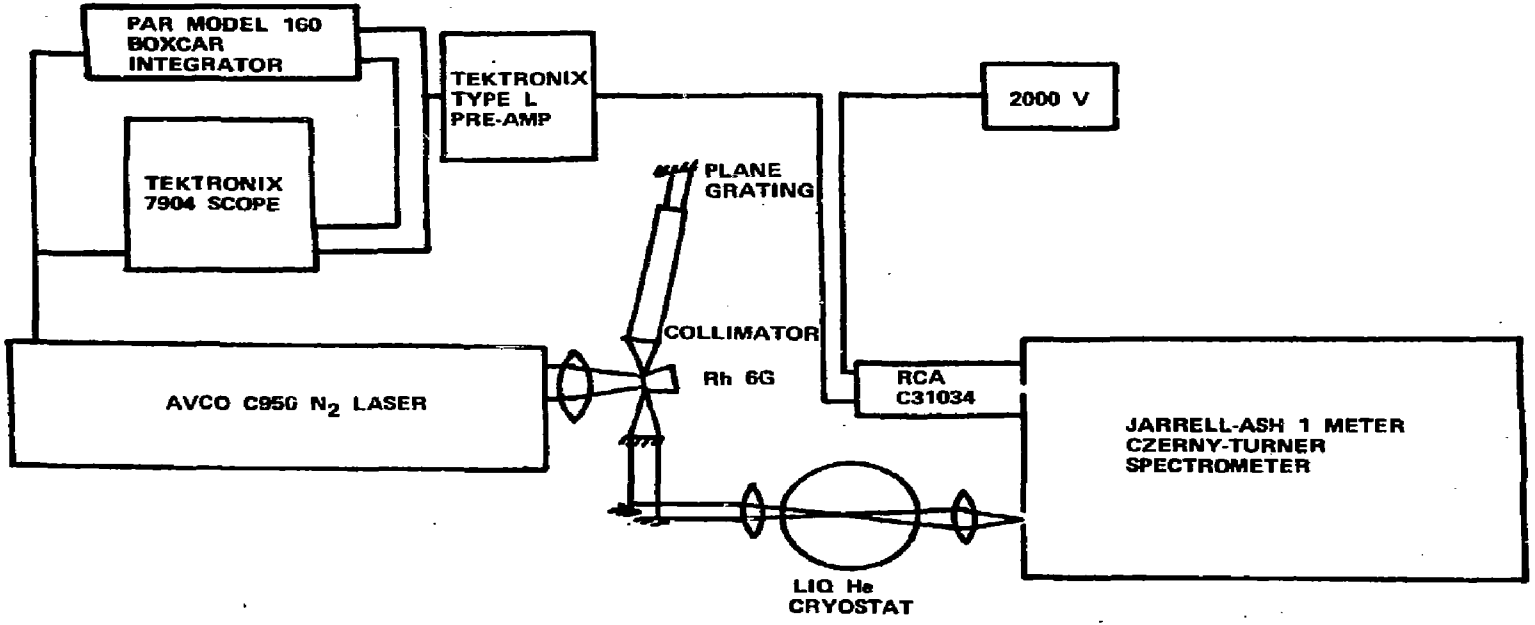
PAR MODEL 160
BOXCAR
INTEGRATOR
TEKTRONIX
TYPE L
PRE-AMP
2000 V
TEKTRONIX
7904 SCOPE
PLANE
GRATING
COLLIMATOR
Rh 6G
AVCO C950 N_2 LASER
RCA
C31034
JARRELL-ASH 1 METER
CZERNY-TURNER
SPECTROMETER
LIQ He
CRYOSTAT

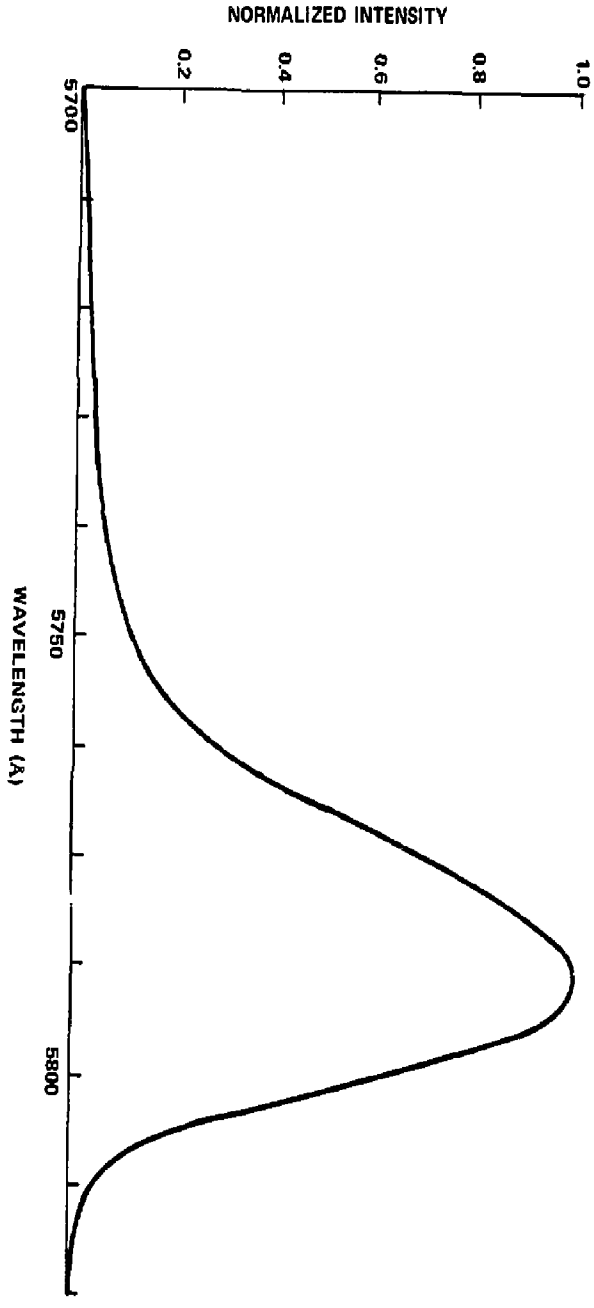
NORMALIZED INTENSITY
0.2
0.4
0.6
0.8
1.0
5700
5750
5800
WAVELENGTH (Å)

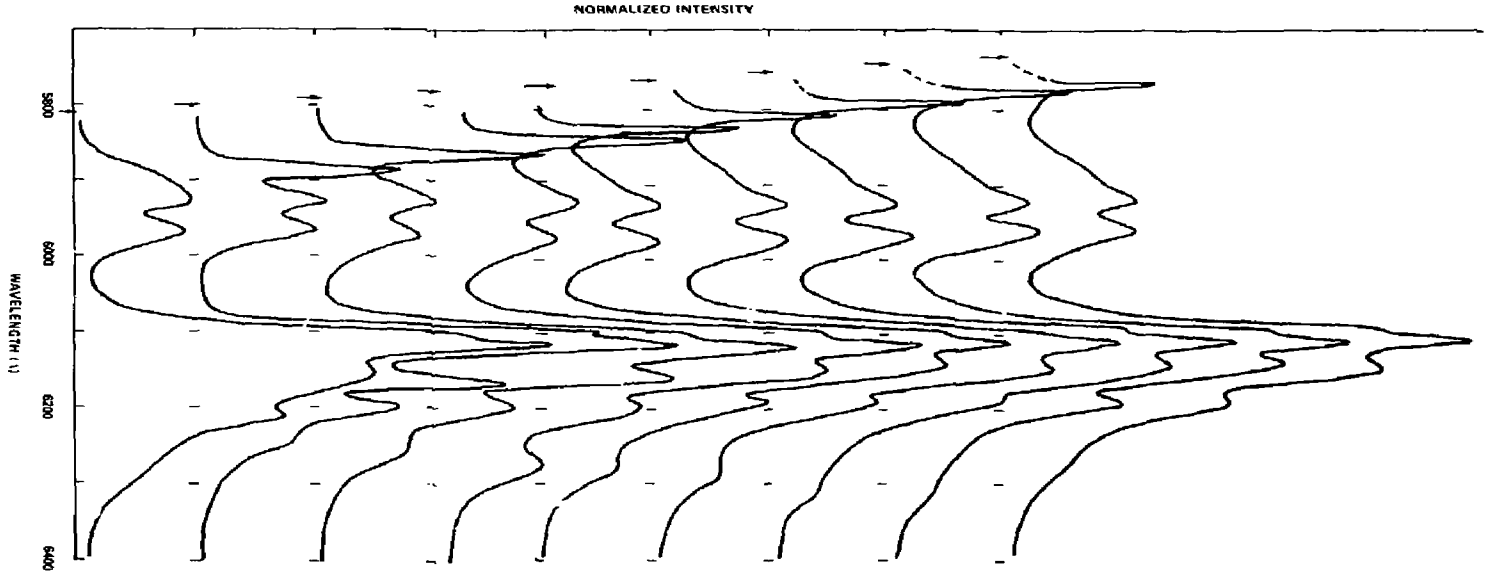
NORMALIZED INTENSITY
WAVELENGTH (Å)
5800
6000
6200
6400

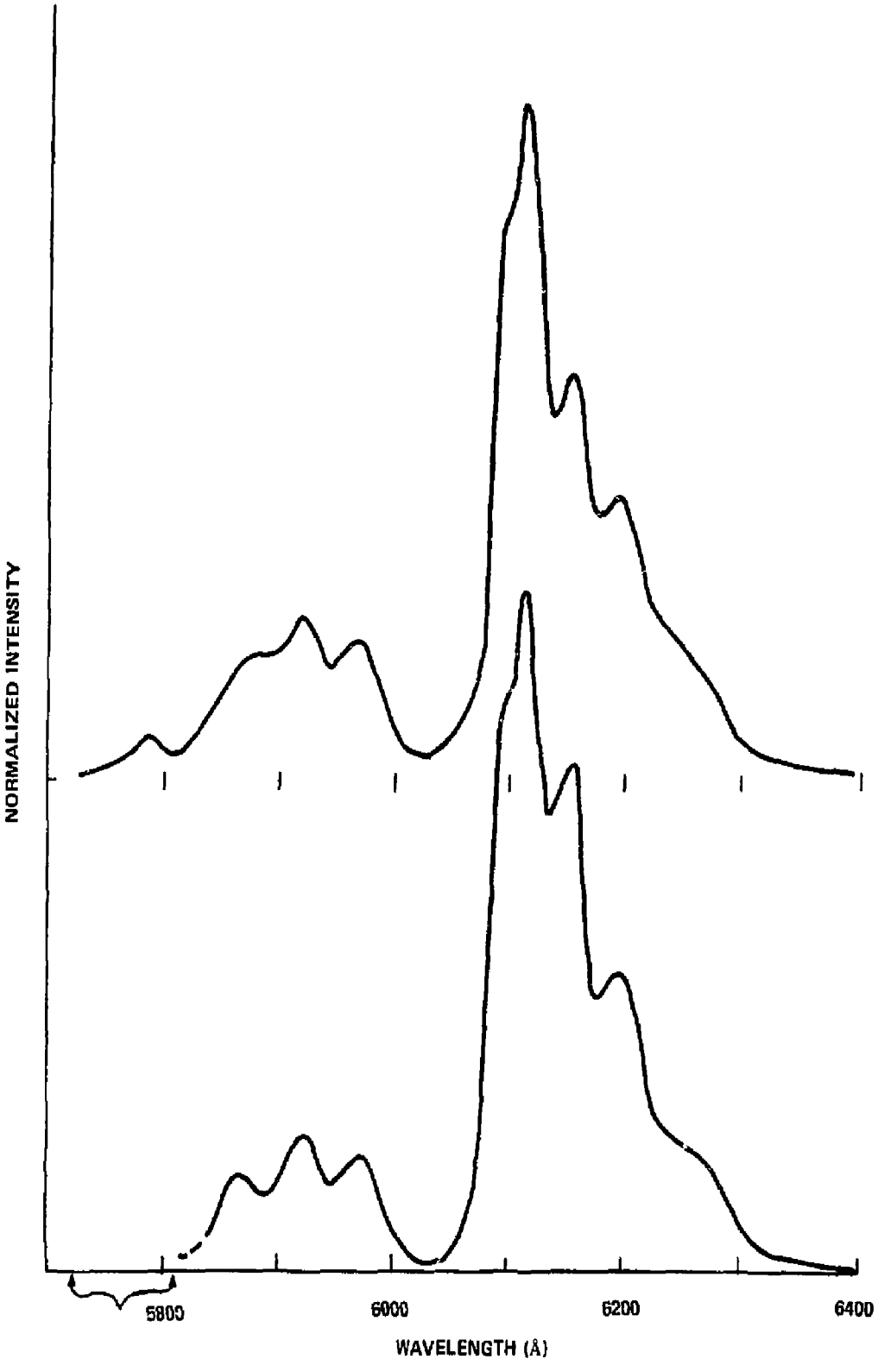
NORMALIZED INTENSITY
5800
6000
6200
6400
WAVELENGTH (Å)

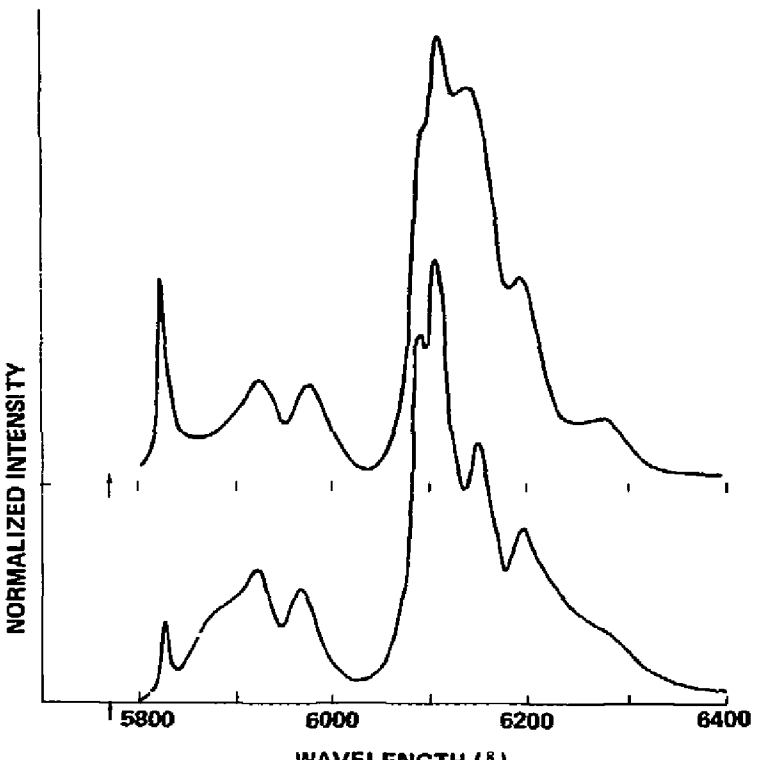
NORMALIZED INTENSITY
5800
6000
6200
6400
WAVELENGTH (Å)

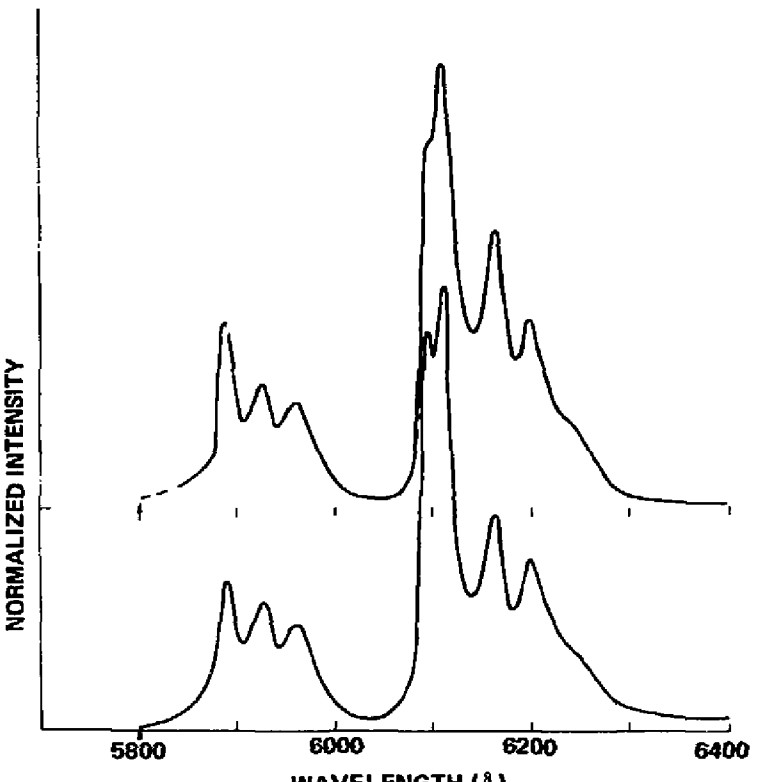
NORMALIZED INTENSITY
5800
6000
6200
6400
WAVELENGTH (Å)

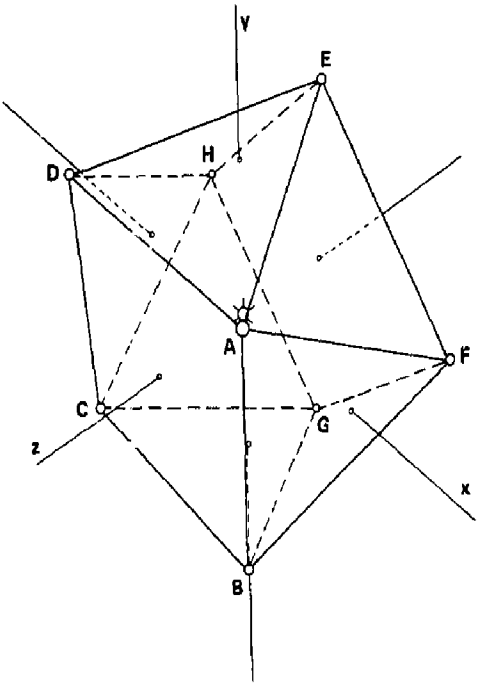
y
E
D
H
A
F
C
G
z
x
B

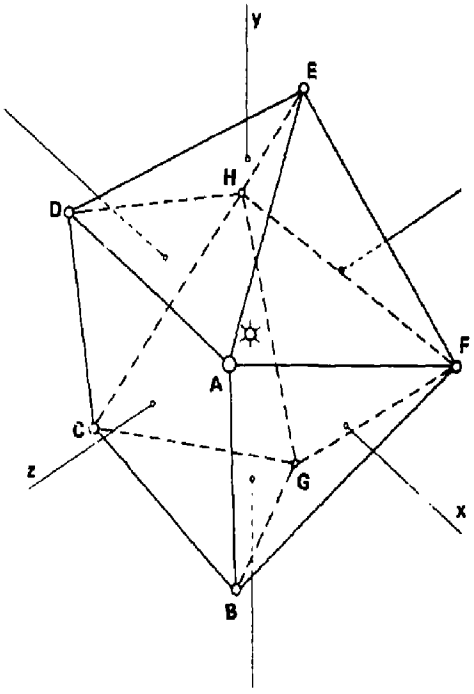
y
E
D
H
A
F
C
G
z
x
B

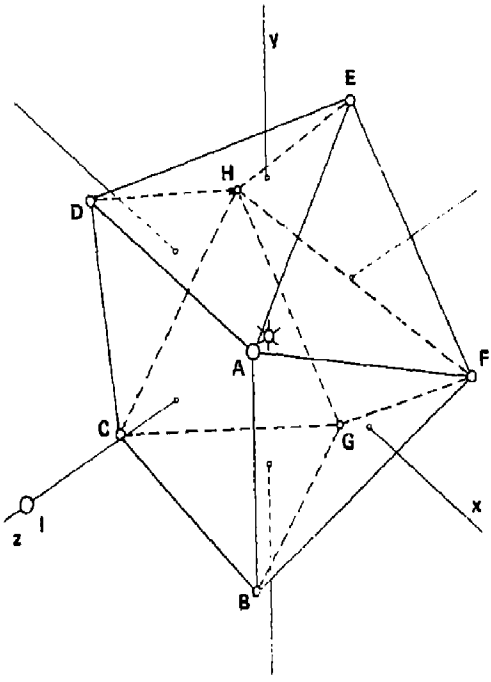
y
E
D
H
A
F
C
G
z
1
x
B

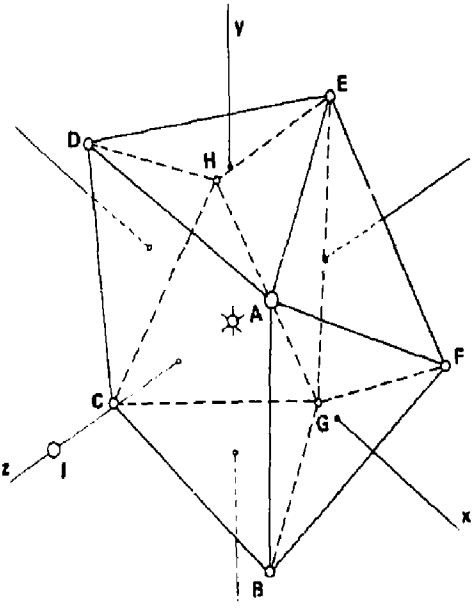
y
E
D
H
A
F
C
G
z
1
x
B

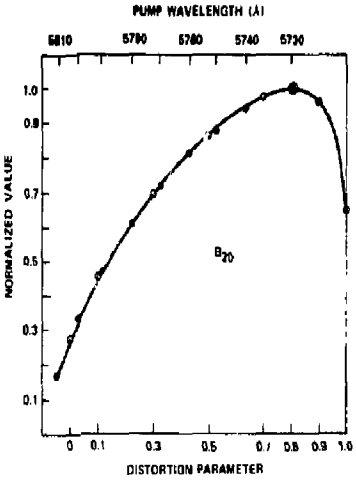
PUMP WAVELENGTH (Å)
5810
5790
5780
5740
5730
NORMALIZED VALUE
1.0
0.9
0.7
0.5
0.3
0.1
B_{20}
0
0.1
0.3
0.5
0.7
0.8
0.9
1.0
DISTORTION PARAMETER

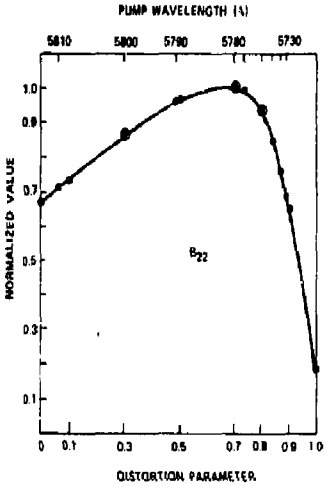
PUMP WAVELENGTH (Å)
5810
5800
5790
5780
5730
NORMALIZED VALUE
1.0
0.9
0.7
0.5
0.3
0.1
B_{22}
0
0.1
0.3
0.5
0.7
0.8
0.9
1.0
DISTORTION PARAMETER

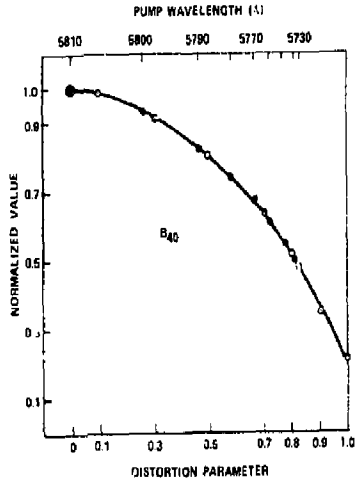
PUMP WAVELENGTH (Å)
5810
5800
5790
5770
5730
NORMALIZED VALUE
1.0
0.9
0.7
0.5
0.1
B_{40}
0
0.1
0.3
0.5
0.7
0.8
0.9
1.0
DISTORTION PARAMETER

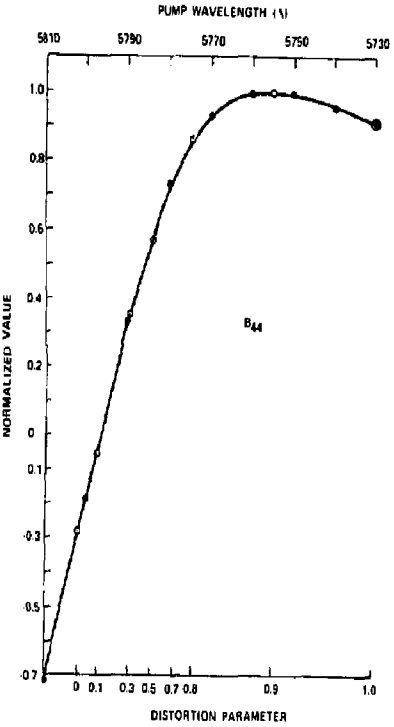
PUMP WAVELENGTH (Å)
5810
5790
5770
5750
5730
NORMALIZED VALUE
1.0
0.8
0.6
0.4
0.2
0
0.1
0.3
0.5
0.7
B_{44}
0
0.1
0.3
0.5
0.7
0.8
0.9
1.0
DISTORTION PARAMETER

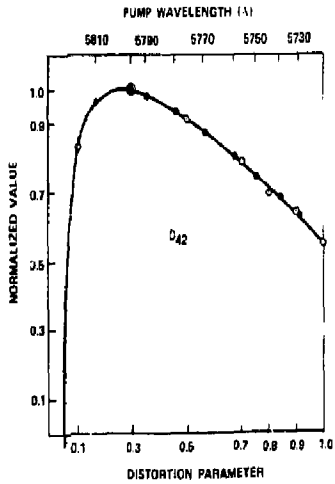
PUMP WAVELENGTH (Å)
5810
5790
5770
5750
5730
NORMALIZED VALUE
1.0
0.9
0.7
0.5
0.3
0.1
D_{42}
0.1
0.3
0.5
0.7
0.8
0.9
1.0
DISTORTION PARAMETER

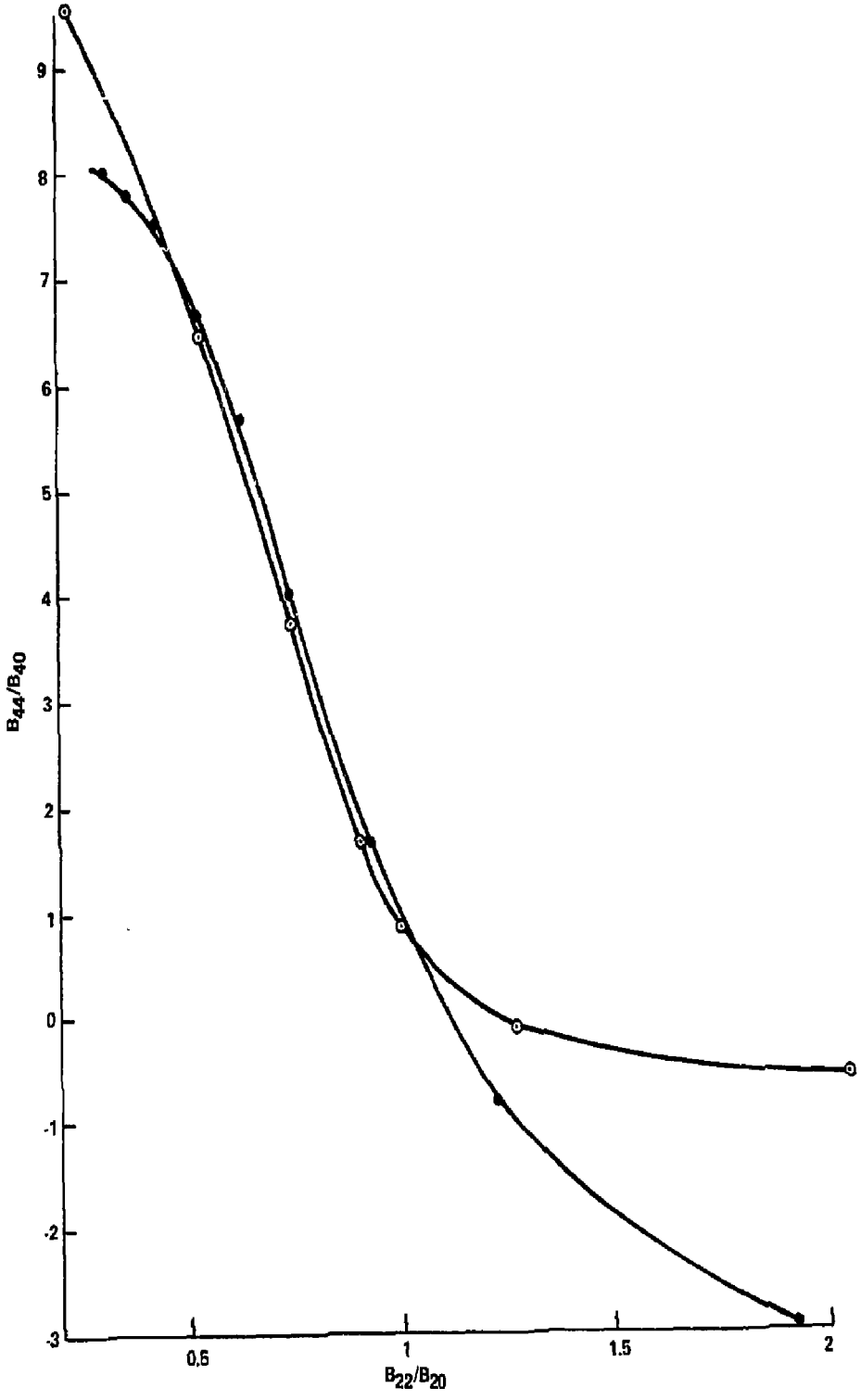
9
8
7
6
5
4
3
2
1
0
-1
-2
-3
B_{44}/B_{40}
0.5
1
1.5
2
B_{22}/B_{20}

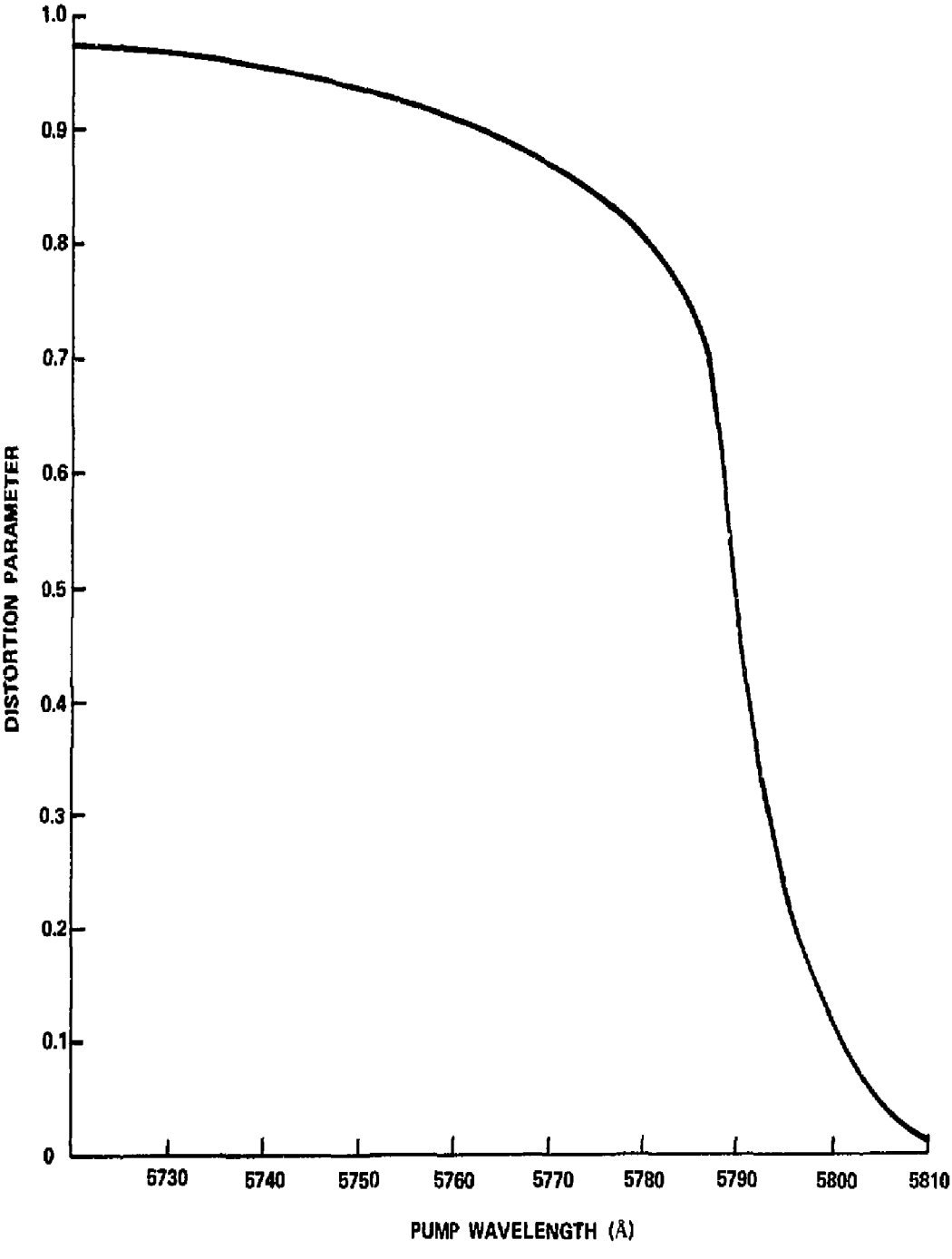
1.0
0.9
0.8
0.7
0.6
0.5
0.4
0.3
0.2
0.1
0
DISTORTION PARAMETER
5730
5740
5750
5760
5770
5780
5790
5800
5810
PUMP WAVELENGTH (Å)

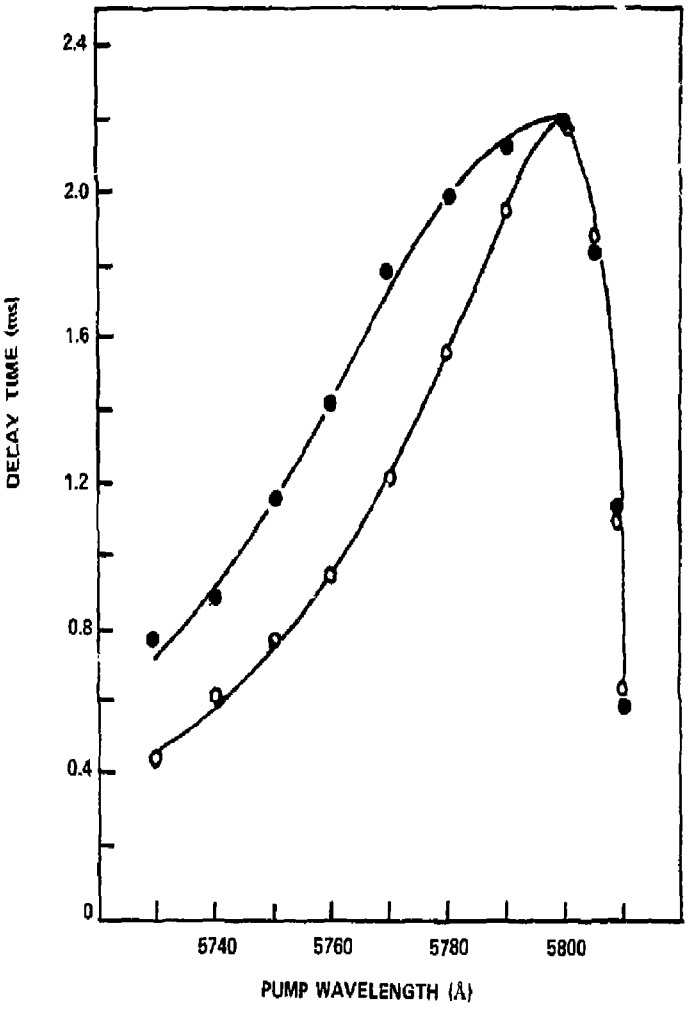
2.4
2.0
1.6
1.2
0.8
0.4
0
DECAY TIME (ms)
5740
5760
5780
5800
PUMP WAVELENGTH (Å)